

UNIVERSIDAD DE CONCEPCIÓN



CENTRO DE INVESTIGACIÓN EN
INGENIERÍA MATEMÁTICA (CI²MA)



**A model of flotation with sedimentation: steady states and
numerical simulation of transient operation**

RAIMUND BÜRGER, STEFAN DIEHL,
MARÍA CARMEN MARTÍ, YOLANDA VÁSQUEZ

PREPRINT 2019-25

SERIE DE PRE-PUBLICACIONES

A MODEL OF FLOTATION WITH SEDIMENTATION: STEADY STATES AND NUMERICAL SIMULATION OF TRANSIENT OPERATION

RAIMUND BÜRGER^{A,*}, STEFAN DIEHL^B, MARÍA DEL CARMEN MARTÍ^C,
AND YOLANDA VÁSQUEZ^A

ABSTRACT. A spatially one-dimensional model of the hydrodynamics of a flotation column is based on one continuous phase, the fluid, and two disperse phases: the aggregates, that is, bubbles with attached hydrophobic valuable particles, and the solid particles that form the gangue. A common feed inlet for slurry mixture and gas is considered and the bubbles are assumed to be fully aggregated with hydrophobic particles as they enter the column. The conservation law of the three phases yields a model expressed as a system of partial differential equations where the nonlinear constitutive flux functions come from the drift-flux and solids-flux theories. In addition, the total flux functions are discontinuous in the spatial (height) coordinate because of two inlets (slurry and wash water) and outlets at the top and bottom. The desired stationary solutions of this model can be characterized by operating charts. A novel numerical method is used for simulations of the hydrodynamics under variable operating conditions such as control actions that drive the process to desired states of operation.

1. INTRODUCTION

1.1. **Scope.** Froth flotation is widely used for the recovery of valuable minerals, such as copper- and lead-bearing minerals, from low-grade ores. This process selectively separates hydrophobic materials (that are repelled by water) from hydrophilic (that would be attracted to water), where both are suspended in a viscous fluid. It is well known that this physico-chemical separation process functions roughly as follows: gas is introduced close to the bottom of a column (see Figure 1), and the bubbles generated rise upward throughout the pulp that contains the solid particles, which can be divided into two main groups. The hydrophobic particles (minerals or ores that should be recovered) attach to the bubbles that float to the top of the column, forming foam or froth carrying the valuable material (the concentrate in mining) that is removed usually through a launder. On the other hand, the hydrophilic particles (slimes or gangue) do not attach to bubbles, but settle to the bottom of the vessel, unless they are trapped in the bulk upflow. Close to the top, additional wash

Date: July 4, 2019.

*Corresponding author.

^ACI²MA and Departamento de Ingeniería Matemática, Facultad de Ciencias Físicas y Matemáticas, Universidad de Concepción, Casilla 160-C, Concepción, Chile. E-Mail: rburger@ing-mat.udec.cl, yvasquez@ci2ma.udec.cl.

^BCentre for Mathematical Sciences, Lund University, P.O. Box 118, S-221 00 Lund, Sweden. E-Mail: stefan.diehl@math.lth.se.

^CDepartament de Matemàtiques, Universitat de València, Av. Vicent Andrés Estellés, E-46100 Burjassot, Spain. E-Mail: María.C.Marti@uv.es.

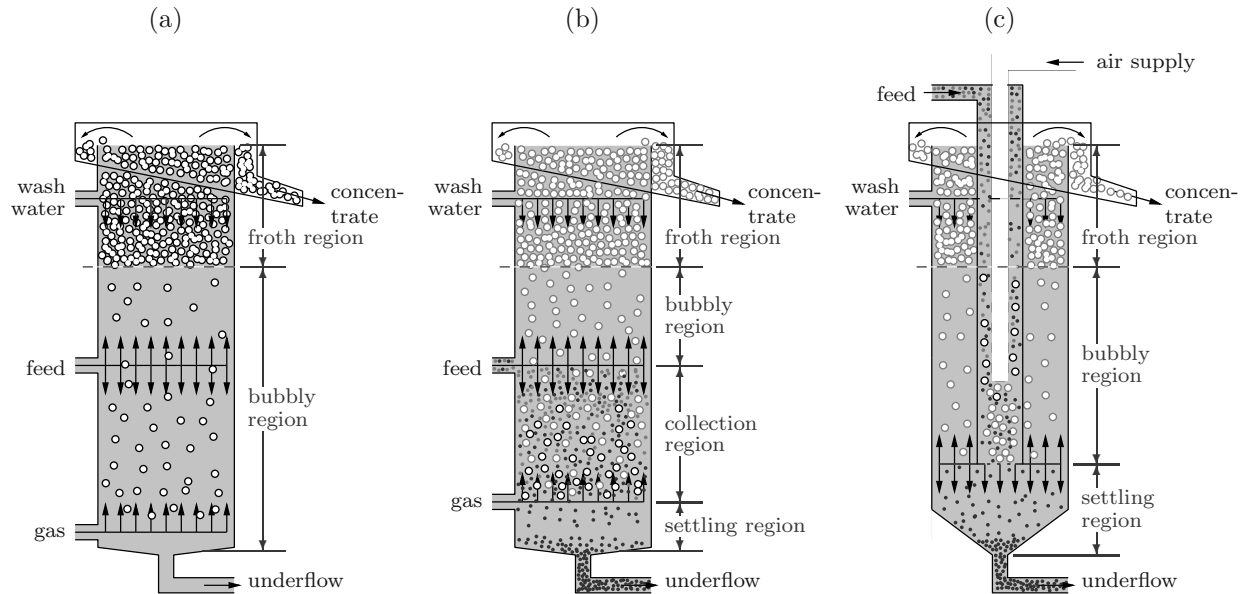


FIGURE 1. Conceptual variants of a flotation column: (a) simplified model of two-phase gas-liquid flow (Bürger et al. 2018a), (b) complete flotation column including a collection region (Finch and Dobby 1990), (c) upper part of the Reflux Flotation Cell by Dickinson and Galvin (2014) and Galvin and Dickinson (2014).

water can be injected to assist with the rejection of entrained impurities (Vandenberghe et al. 2005) and to increase the froth stability and improve recovery (Finch and Dobby 1990; Pal and Masliyah 1989). Mathematical models are required for the design, simulation, and eventually control of flotation columns.

Motivated by Stevenson et al. (2008), Dickinson and Galvin (2014) and Galvin and Dickinson (2014), Bürger et al. (2018a) presented a one-dimensional two-phase model describing only the movement of gas bubbles and fluid. The flotation column modelled in that work has a separate gas inlet near the bottom, which is commonly used in mineral processing so that a collection zone is created in which the hydrophobic particles attach to the gas bubbles inside the column. Other devices have a common feed inlet for both slurry and gas bubbles, so that the aggregation process (the attachment of hydrophobic particles to bubbles) mostly occurs in the inlet pipe. Here, we model such a column (see Figure 1 (c)) and assume that the bubbles are fully loaded with hydrophobic particles as the mixture enters the column, so that the aggregation process is concluded when particles and bubbles enter the column.

The governing equation of the two-phase model studied by Bürger et al. (2018a) is a scalar, quasilinear first-order partial differential equation (known as conservation law; see, e.g., LeVeque (1992) or Holden and Risebro (2015) for the background). A non-standard ingredient of this model is a flux function that is discontinuous at several spatial positions due to the feed sources of gas, slurry, and wash water, and the lower and upper outlets of tailings and concentrate. This formulation was recently extended (Bürger et al. 2019)

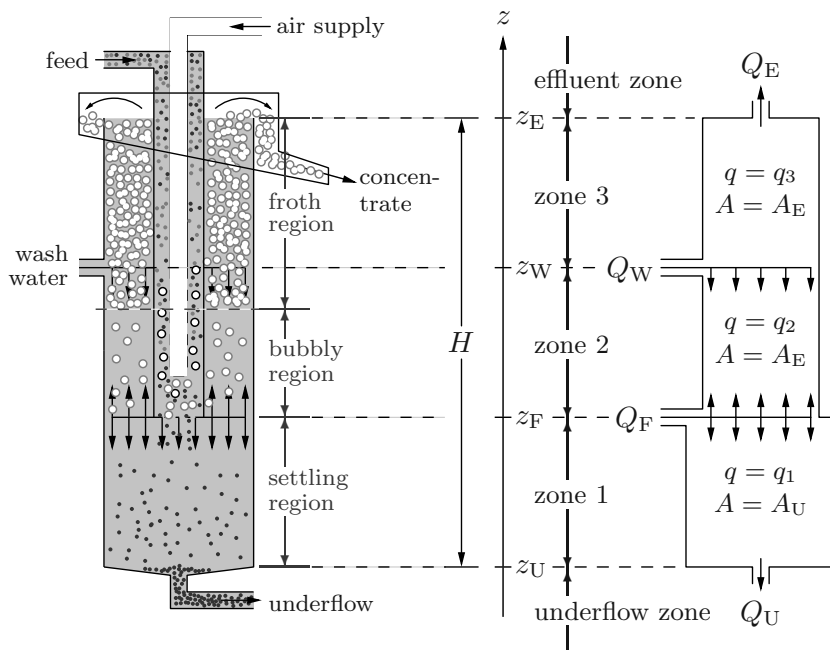


FIGURE 2. Left: Schematic of a flotation column with non-constant cross-sectional area $A(z)$ (A_U below and A_E above the feed level) utilized for numerical simulations in this paper. Right: corresponding one-dimensional conceptual model. The unit is fed with wash water at level $z = z_W$ and a mixture of aggregates and feed slurry at $z = z_F$, where $z_U < z_F < z_W < z_E$ divide the real line into the zones inside the column and the underflow and effluent zones. The corresponding volumetric feed flows of wash water, $Q_W \geq 0$, and of feed slurry, $Q_F > 0$, are given functions of time, as is the volumetric underflow rate $Q_U \geq 0$. The resulting effluent volumetric overflow $Q_E = Q_W + Q_F - Q_U$ is assumed to be nonnegative, $Q_E \geq 0$, so that the mixture is conserved and the vessel is always completely filled with mixture.

to a three-phase model that also includes the settling of solid particles within the flotation column. The three-phase flow of solids, gas (bubbles or aggregates) and fluid is modelled in one space dimension. We herein utilize that same model of (Bürger et al. 2019) and present new numerical results relevant to applications. The governing partial differential equations (PDEs) can be written as the system

$$A(z) \frac{\partial \phi}{\partial t} + \frac{\partial}{\partial z} (A(z) J(\phi, z, t)) = Q_F(t) \phi_F(t) \delta(z - z_F), \quad (1.1a)$$

$$A(z) \frac{\partial}{\partial t} ((1 - \phi)\varphi) - \frac{\partial}{\partial z} (A(z) F(\varphi, \phi, z, t)) = Q_F(t) \phi_{s,F}(t) \delta(z - z_F), \quad (1.1b)$$

where the independent variables are time $t > 0$ and height z . The unknowns are the volume fraction of aggregates ϕ and the volume fraction of solids in the solid-liquid suspension

$$\varphi = \frac{\phi_s}{1 - \phi},$$

where ϕ_s is the volume fraction of (hydrophilic) solids and $1 - \phi$ is the volume fraction of the suspension outside the aggregates. This means that if a small volume V is given, then φ is the ratio of the volume occupied by the solids $\phi_s V$ and the volume occupied by the suspension $(1 - \phi)V$.

Both unknowns ϕ and φ are functions of z and t . The given flux functions $J(\phi, z, t)$ and $F(\varphi, \phi, z, t)$, whose precise definition will be made explicit later, involve nonlinear constitutive functions of ϕ and φ that describe the rise of bubbles and settling of solids. The fluxes J and F are discontinuous in z at several positions (namely at $z = z_U, z_F, z_W$ and z_E ; see Figure 2) associated with singular feed sources, the underflow and the effluent, and in general depend on t through the control of in- and outflows. The possibly varying cross-sectional area is denoted by $A(z)$. The right-hand sides of the equations contain the Dirac function and given positive feed volume fractions of the aggregates ϕ_F and solids $\phi_{s,F}$. The model is complete with initial conditions and no boundary conditions are required: the bounds of the vessel at $z = z_U$ and $z = z_E$ are captured by discontinuities of $J(\phi, z, t)$ and $F(\varphi, \phi, z, t)$.

In this contribution, we summarize from Bürger et al. (2019) the derivation of (1.1), the new numerical method, and give example on control actions for obtaining desired steady states. These are time-independent (stationary) solutions of (1.1). Among the variety of theoretically possible steady states we select those for discussion that are most relevant for practical applications, namely those that have a high concentration of aggregates at the top, the foam, and no bubbles at the lower part of the column, and conversely for the solids gangue. These steady states represent the stationary modes of operation of a flotation column without changing control parameters. It turns out that such desired steady states need some wash water to be injected, i.e., $Q_W > 0$. We provide conditions (for steady-state operation) on how much wash water can be used to be efficient, i.e., how much can flow down through the foam. Applying more wash water will only mean that it is wasted through the effluent.

Both transient and stationary solutions have layers of different concentrations of bubbles (foam) and particles separated by discontinuities in concentration. Equation (1.1a) depends only on the unknown ϕ . Our approach is to solve each equation locally as a scalar conservation law with discontinuous flux. The feasible steady states relevant for operation in real applications can be visualized by so-called *operating charts* that illustrate the necessary constraints for the control of the volumetric flows. Moreover, Bürger et al. (2019) advanced a numerical scheme for (1.1) that produces approximate solutions that take physically relevant values only (volume fractions between zero and one). It is the purpose of this paper to demonstrate that the model and numerical scheme provide a useful tool for the simulation of the operation of a flotation column in the case of a common feed inlet of the three phases and when no aggregation occurs in the column. In particular, responses of the unit to changes in operating conditions (such as the rates and composition of feed flows) are illustrated.

1.2. Related work. The two-phase flow of rising bubbles in a liquid has often been modelled by the drift-flux theory by Wallis (1969), see, e.g., (Rietema 1982; Yianatos et al. 1986; Dobby et al. 1988; Langberg and Jameson 1992; Cruz 1997; Brennen 2005; Vandenberghe et al. 2005; Ireland and Jameson 2007; Stevenson et al. 2008; Dickinson and Galvin 2014; Galvin and Dickinson 2014; Galvin et al. 2014). The theory considers the relationships between the nonlinear flux of bubbles relative to the fluid (denoted here the batch drift flux) and the applied bulk flows that arise due to the inlets and outlets of the column. The drift-flux theory means a rigorous way of investigating the hydrodynamics in one dimension; however, it is applicable under steady-state conditions only. In this way Stevenson et al. (2007) analysed steady-state conditions for settling gangue in foam.

As pointed out by Stevenson et al. (2008), the flotation column shown in Figure 2 with one inlet of gas and fluid (or suspension) works in principle as an inverted clarifier-thickener used for continuous sedimentation of a solid-liquid suspension. The corresponding theory for sedimentation for particles in a liquid started with Kynch (1952) and is often denoted the solids-flux theory (Diehl 2001, 2008). This theory is well developed and has given rise to models of continuous sedimentation described by scalar conservation laws with discontinuous flux along with several extensions to account, for example, for sediment compressibility. The authors' contributions to original mathematical research on this class of models include Bürger et al. (2004, 2005, 2010, 2013, 2018b) and Diehl (1996, 2001, 2005). The model of flotation proposed herein is based on this experience.

The one-dimensional formulation chosen here has the advantage that only equations for the gas and solids concentrations need to be solved, while two- or three-dimensional formulations invariably require solving additional equations for the flow of the mixture. However, the one-dimensional setting requires to describe the feed mechanism and diverging bulk flows by discontinuities with respect to z in the definitions of F and J . These abrupt changes, in combination with the nonlinearities of these functions that arise from constitutive functions arising from the drift- and solid-flux theories, cause the principal mathematical difficulty for the construction of connections of ϕ -, φ - and ϕ_s -values across jumps in the definitions of F and J . An in-depth discussion of these mathematical issues along with a comprehensive analysis and detailed descriptions on how to obtain and categorize the steady states are given in our previous work; see Bürger et al. (2019).

To the authors' knowledge, the flotation columns have not yet been described by partial differential equations that would be based on these theories developed since the 1990s. Bascur (1991) noticed that his two-phase framework could be used for both solid-liquid and gas-liquid separation processes. Several aspects of modelling a flotation column are provided by Cruz (1997), who also reviewed earlier works. Tian et al. (2018) advance a hyperbolic system that includes the attachment process; however, they assume that the flux functions are linear. In particular, their approach does not constitute an extension of the drift or solids flux theories, in contrast to ours. While the vast majority of references to flotation processes are related to mineral processing, we mention that flotation processes are also used for removing other small particles, oil droplets, printing ink and organic matter in diverse processes such as wastewater treatment (Rubio et al. 2002).

1.3. Outline of the paper. The remainder of the paper is organized as follows. The mathematical model is outlined in Section 2, starting with some general assumptions (in Section 2.1) and a description of the batch-drift and batch-settling flux functions (Section 2.2), which introduce nonlinearity into the fluxes J and F . Then, in Section 2.3, we outline the derivation of the governing equations (1.1) from the conservation of mass equations of the gas (aggregates), the solid and the fluid. The existence of stationary and transient solutions depends on geometric properties of the nonlinear flux functions, such as the locations of extrema and inflection points, which are outlined in Section 2.4. In Section 3, the most desired steady states and their characterization are presented. We extract in Section 3.1 the most interesting and usable results. The most desired steady states and their *operating charts* for given values on ϕ_F and $\phi_{s,F}$ are presented in Section 3.2. In Section 4 we present numerical solutions of (1.1) that illustrate the transient behaviour of the model. (The numerical method is detailed in Bürger et al. (2019) and is summarized in the Appendix of this paper.) After stating some preliminaries (in Section 4), we present in Sections 4.2 to 4.4 three examples of simulations that illustrate the model predictions, in particular the formation of and transitions between steady states and the response of the system to changes of operating conditions.

2. MATHEMATICAL MODEL

2.1. Assumptions. Figure 2 shows the flotation column studied in this paper and introduces the distinguished heights z_U , z_F , z_W and z_E along with the associated volume flows Q_U , Q_F , Q_W and Q_E .

To model a feed inlet pipe located in the upper part and centre of a cylindrical column, the cross-sectional area $A = A(z)$ is assumed to have a discontinuity at the feed inlet (Figure 2):

$$A(z) := \begin{cases} A_E & \text{for } z \geq z_F, \\ A_U & \text{for } z < z_F, \end{cases} \quad \text{where } A_E \leq A_U. \quad (2.1)$$

We mention that our numerical method can handle any other variation in the cross-sectional area, for example, a conical bottom as shown in 1.

We distinguish three phases: the *fluid phase* (index f), the *solid phase* (index s), which models solid particles that are suspended in the fluid, and the *aggregate phase* (index a), which models gas bubbles fully loaded with hydrophobic particles. We let $\phi_i = \phi_i(z, t)$ denote the volume fraction of phase $i \in \{a, f, s\}$, where $\phi_a + \phi_f + \phi_s \equiv 1$. The maximum volume fraction for any phase is one. In what follows, we will use the simpler notation $\phi := \phi_a$; cf. (1.1). Furthermore, we assume constant phase densities $\rho_a < \rho_f < \rho_s$, consistently with the assumption that bubbles rise (float) and particles settle (sink). Finally, the aggregate bubbles and the solid particles are assumed to be monosized. We also suppose that gas bubbles do not coalesce or break.

2.2. Batch-drift- and batch-settling-flux functions. The drift-flux and the solids-flux theories stipulate a batch-drift-flux function $j_b(\phi)$ and a batch-settling-flux function $f_b(\varphi)$, respectively:

$$j_b(\phi) = \phi v_{\text{term},a} V_a(\phi), \quad (2.2)$$

$$f_b(\varphi) = \varphi v_{\text{term},s} V_s(\varphi), \quad (2.3)$$

where $v_{\text{term},a}$ and $v_{\text{term},s}$ are the terminal velocities of a single aggregate and a single solid particle, respectively, in an unbounded fluid. The discussion of these quantities is beyond our focus (but see Stevenson et al. 2008); here it suffices to assume that $v_{\text{term},a} > 0$ and $v_{\text{term},s} > 0$ are set constants for a given material. Furthermore, the dimensionless hindered bubbling and settling functions, V_a and V_s respectively, satisfy $V_a(0) = V_s(0) = 1$ and are often given by the Richardson-Zaki (1954) expression

$$\begin{aligned} V_a(\phi) &= (1 - \phi)^{n_a} \quad \text{for } 0 \leq \phi \leq 1, n_a \geq 0, \\ V_s(\varphi) &= (1 - \varphi)^{n_s} \quad \text{for } 0 \leq \phi \leq 1, n_s \geq 1. \end{aligned} \quad (2.4)$$

Realistic values of the parameter n_a range from 2 to 3.2 (Dickinson and Galvin 2014; Galvin and Dickinson 2014; Pal and Masliyah 1989; Vandenberghe et al. 2005). We use $n_a = 3.2$ and $v_{\text{term},a} = 2.7$ cm/s for all plots and simulations in the present article along with $n_s = 2.5$ (Dickinson and Galvin 2014) and $v_{\text{term},s} = 0.5$ cm/s.

Outside the flotation column, we assume that all three phases have the same velocity. Mathematically, this means that our problem can be defined on the real line z with $j_b = f_b = 0$ for $z < z_U$ and $z > z_E$.

2.3. Derivation of governing equations. Conservation of mass for each phase implies the following system of balance equations,

$$\frac{\partial}{\partial t}(A(z)\phi) + \frac{\partial}{\partial z}(A(z)\phi v_a) = Q_F \phi_F \delta(z - z_F), \quad (2.5)$$

$$\frac{\partial}{\partial t}(A(z)\phi_s) + \frac{\partial}{\partial z}(A(z)\phi_s v_s) = Q_F \phi_{s,F} \delta(z - z_F), \quad (2.6)$$

$$\frac{\partial}{\partial t}(A(z)\phi_f) + \frac{\partial}{\partial z}(A(z)\phi_f v_f) = Q_F \phi_{f,F} \delta(z - z_F) + Q_W \phi_{f,W} \delta(z - z_W), \quad (2.7)$$

where the right-hand sides contain Dirac functions, volumetric flows and the incoming volume fractions of aggregates ϕ_F , solids $\phi_{s,F}$ and fluid $\phi_{f,W} \equiv 1$. We assume that $\phi_F + \phi_{s,F} + \phi_{f,F} \equiv 1$ with $0 < \phi_F, \phi_{s,F}, \phi_{f,F} < 1$. In terms of the volume-average velocity, or bulk velocity, of the mixture $q := \phi v_a + \phi_s v_s + \phi_f v_f$, the sum of (2.5)–(2.7) can be written as

$$\frac{\partial}{\partial z}(A(z)q) = Q_F \delta(z - z_F) + Q_W \delta(z - z_W). \quad (2.8)$$

Consequently, in the flotation column q varies with height z because of the two inlet flows and (2.1). Since $A(z)q(z, t) = -Q_U(t)$ for $z < z_F$, we can integrate (2.8) to obtain

$$q(z, t) = \begin{cases} q_1 := -Q_U/A_U & \text{in the underflow zone and zone 1,} \\ q_2 := (-Q_U + Q_F)/A_E & \text{in zone 2,} \\ q_3 := (-Q_U + Q_F + Q_W)/A_E & \text{in zone 3 and the effluent zone.} \end{cases} \quad (2.9)$$

Hence, this identity replaces (2.7), and we will next rewrite the fluxes ϕv_a and $\phi_s v_s$ in (2.5) and (2.6) in terms of q and two constitutive functions j_b and f_b . Both can be expressed by

relative velocities. We denote the volume-average velocity, or bulk velocity, of the solid-fluid suspension by

$$q_{\text{sus}} := \frac{\phi_{\text{s}}v_{\text{s}} + \phi_{\text{f}}v_{\text{f}}}{\phi_{\text{s}} + \phi_{\text{f}}} = \varphi v_{\text{s}} + (1 - \varphi)v_{\text{f}}.$$

Then we define the aggregate-suspension relative velocity $u_{\text{asus}} := v_{\text{a}} - q_{\text{sus}} = v_{\text{a}} - \varphi v_{\text{s}} - (1 - \varphi)v_{\text{f}}$ and the solid-fluid relative velocity $u_{\text{sf}} := v_{\text{s}} - v_{\text{f}}$. From the definitions of q_{sus} , u_{asus} and u_{sf} , we derive that

$$v_{\text{a}} = q + (1 - \phi)u_{\text{asus}}, \quad (2.10)$$

$$v_{\text{s}} = q + (1 - \varphi)u_{\text{sf}} - \phi u_{\text{asus}}. \quad (2.11)$$

We assume that u_{asus} is a function of ϕ and u_{sf} is a function of φ . Considering a closed column ($q = 0$), we obtain by comparing (2.10) with (2.2) that

$$\phi(1 - \phi)u_{\text{asus}} = j_{\text{b}}(\phi),$$

while considering a closed column ($q = 0$) with no bubbles ($\phi = 0$), we obtain by comparing (2.11) with (2.3) that

$$\varphi(1 - \varphi)u_{\text{sf}} = -f_{\text{b}}(\varphi),$$

where $f_{\text{b}} \geq 0$ in the downwards direction of sedimentation, while by definition $u_{\text{sf}} > 0$ in the upwards z -direction. It is possible to obtain the following expressions:

$$\phi v_{\text{a}} = \phi q + j_{\text{b}}(\phi) =: J(\phi, z, t),$$

$$\phi_{\text{s}}v_{\text{s}} = (1 - \phi)\varphi q - (1 - \phi)f_{\text{b}}(\varphi) - \varphi j_{\text{b}}(\phi) =: -F(\varphi, \phi, z, t),$$

where the minus sign is to have F positive in the direction of sedimentation. Inserting these expressions into (2.5) and (2.6) we get a system of PDEs within a zone. To get the governing PDE system (1.1), we assume that in the under- and overflow zones, all phases are assumed to have the same velocity, i.e., u_{asus} and u_{sf} are zero, so we set $j_{\text{b}} := 0$ and $f_{\text{b}} := 0$ in these zones. The total flux functions in (1.1) are thus given by

$$J(\phi, z, t) = \begin{cases} j_{\text{E}}(\phi, t) := q_3(t)\phi & \text{in the effluent zone,} \\ j_3(\phi, t) := q_3(t)\phi + j_{\text{b}}(\phi) & \text{in zone 3,} \\ j_2(\phi, t) := q_2(t)\phi + j_{\text{b}}(\phi) & \text{in zone 2,} \\ j_1(\phi, t) := q_1(t)\phi + j_{\text{b}}(\phi) & \text{in zone 1,} \\ j_{\text{U}}(\phi, t) := q_1(t)\phi & \text{in the underflow zone,} \end{cases}$$

$$F(\varphi, \phi, z, t) = \begin{cases} f_{\text{E}}(\varphi, \phi, t) := -(1 - \phi)q_3(t)\varphi & \text{in the effluent zone,} \\ f_3(\varphi, \phi, t) & \text{in zone 3,} \\ f_2(\varphi, \phi, t) & \text{in zone 2,} \\ f_1(\varphi, \phi, t) & \text{in zone 1,} \\ f_{\text{U}}(\varphi, \phi, t) := -(1 - \phi)q_1(t)\varphi & \text{in the underflow zone,} \end{cases}$$

where

$$f_k(\varphi, \phi, t) := (1 - \phi)f_{\text{b}}(\varphi) + (j_{\text{b}}(\phi) - (1 - \phi)q_k(t))\varphi$$

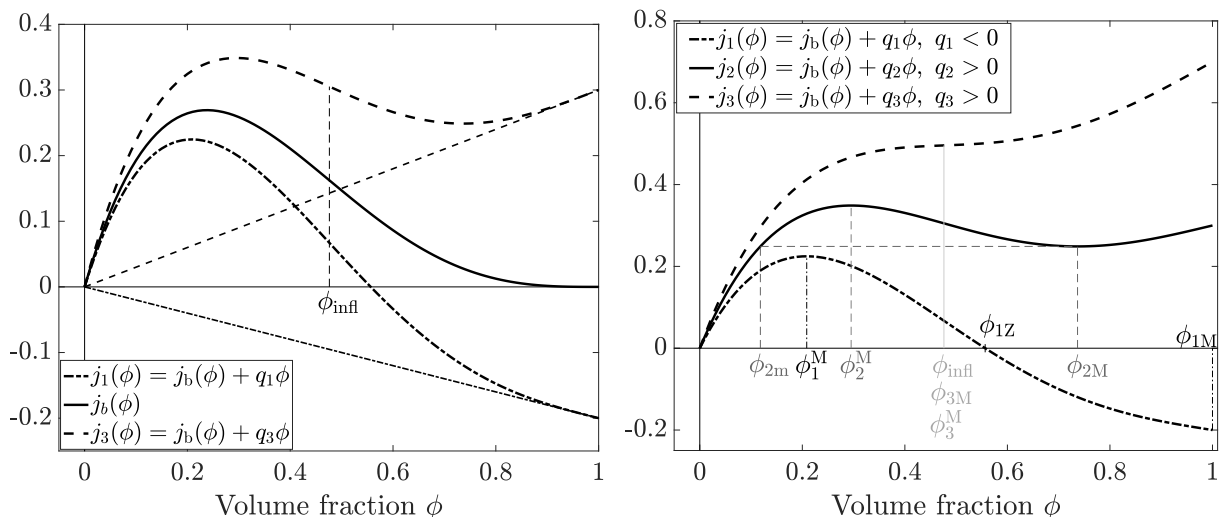


FIGURE 3. Flux functions of the aggregate phase and specific volume fractions. Left: Drift-flux function j_b and flux curves for zones 1 and 3. Right: In dark gray colour, the local minimum ϕ_{2M} and appurtenant ϕ_{2m} for the flux j_2 in zone 2 where $q_2 > 0$. In black colour, the local maximum ϕ_1^M and zero ϕ_{1Z} for flux j_1 with $q_1 < 0$. In light gray, we have represented a zone flux j_3 with a relatively high value of $q_3 > 0$, so that $\phi_{3M} = \phi_3^M = \phi_{\text{infl}}$. In these and other plots, we have used the expression (2.4) with $n_a = 3.2$ in the drift-flux function j_b . The unit on the vertical axis is cm/s.

$$= (1 - \phi)f_b(\varphi) + (j_k(\phi, t) - q_k(t))\varphi, \quad k = 1, 2, 3.$$

2.4. Properties of the flux functions. The drift-flux and settling-flux functions j_b and f_b are assumed to have similar qualitative properties, namely the following; see Figure 3. We assume that $j_b(0) = j_b(1) = 0$ and there exists precisely one inflection point ϕ_{infl} such that $j_b''(\phi) < 0$ for $0 \leq \phi < \phi_{\text{infl}}$ and $j_b''(\phi) > 0$ for $\phi_{\text{infl}} \leq \phi < 1$. We also assume that $j_b'(1) = 0$. In particular, these assumptions are satisfied for the fluxes (2.2) and (2.3) and the Richardson-Zaki expression (2.4).

The zone flux functions, j for the aggregates and $f(\cdot, \phi)$ for the solids, have an additional linear term due to the bulk velocity of the zone. We temporarily skip the time dependence and let $j(\phi) = j_b(\phi) + q\phi$ denote a general zone flux function. (The case for the settling zone flux function $f(\cdot, \phi)$ is similar; however, with an additional dependence on ϕ .) The flux function j has the following distinguished values (exact definitions are given in Burger et al. (2019)):

- The flux $j(\phi)$ has the same inflection point ϕ_{infl} as $j_b(\phi)$ for any value of q .
- If $j(\phi)$ has a zero in the interval $(0, 1)$, which happens only for $q < 0$, we denote it by $\phi_Z = \phi_Z(q)$. If $j(\phi) < 0$ for all $\phi \in (0, 1]$, we set $\phi_Z := 0$.

- There is a local minimum point $\phi_M = \phi_M(q)$ in the interval $(\phi_{\text{infl}}, 1)$, which decreases with increasing $q > 0$ until ϕ_M reaches the inflection point. For higher values of q , $j(\phi)$ is an increasing function and we define $\phi_M := \phi_{\text{infl}}$. For $q < 0$, we set $\phi_M := 1$.
- Given ϕ_M and $q \geq 0$, we define $\phi_m = \phi_m(q)$ as the unique value satisfying

$$j(\phi_m) = j(\phi_M), \quad \text{where } 0 \leq \phi_m \leq \phi_{\text{infl}}. \quad (2.12)$$

- For realistic values of q , there is a local maximum $\phi^M = \phi^M(q)$ in the interval $[0, \phi_{\text{infl}}]$.

Sometimes we write out the dependence on q of the flux function, i.e. $j(\phi; q)$ and $f(\varphi, \phi; q)$.

3. STEADY STATES

3.1. Desired steady states. Generally, a steady-state solution consists of piecewise constant values of ϕ and φ (or, equivalently ϕ_s), generally with discontinuities at the locations of the inlet and outlets, and in each zone there is at most one discontinuity. We are only interested in the desired steady states that have a high concentration of aggregates at the top, so that a layer of foam exists, and zero at the bottom. The hydrophilic solids should settle directly and be present only below the feed level. The different steady states depend on the values of the feed input volume fractions of the aggregates ϕ_F and the solids $\phi_{s,F}$, and on the volumetric flow rates Q_F , Q_U and Q_W . There are several equalities and inequalities involving these variables and the nonlinear flux functions j_b and f_b . We will state the conditions that are needed here and refer to Bürger et al (2019) for all details. Theoretically, there exist many steady states; however, a main conclusion is that all desired steady states that should be able to exist also for small volumetric feed flows Q_F require wash water, i.e., $Q_W > 0$. It turns out that the following desired aggregate steady states are possible for a range of volumetric flows down to zero. They differ only in zone 2, where the solution can be constant low (SSl), constant high (SSh), or have a discontinuity separating these two values (SSd):

$$\phi_{\text{SSl}}(z) := \begin{cases} \phi_E = A_E j_3(\phi_3)/Q_E \geq \phi_{3M} & \text{in the effluent zone,} \\ \phi_3 = \phi_{3M} \geq \phi_2 & \text{in zone 3,} \\ \phi_2 \in [\phi_{2m}, \phi_2^M] & \text{in zone 2,} \\ 0 & \text{in zone 1 and the underflow zone,} \end{cases} \quad (3.1)$$

$$\phi_{\text{SSh}}(z) := \begin{cases} \phi_E = A_E j_3(\phi_3)/Q_E \geq \phi_{3M} & \text{in the effluent zone,} \\ \phi_3 = \phi_{3M} \geq \phi_2 & \text{in zone 3,} \\ \phi_2 \in [\phi_2^M, \phi_{2M}] & \text{in zone 2,} \\ 0 & \text{in zone 1 and the underflow zone,} \end{cases} \quad (3.2)$$

$$\phi_{\text{SSd}}(z) := \begin{cases} \phi_E = A_E j_3(\phi_3)/Q_E \geq \phi_{3M} & \text{in the effluent zone,} \\ \phi_3 = \phi_{3M} & \text{in zone 3,} \\ \phi_2^\uparrow \in [\phi_2^M, \phi_{2M}] & \text{for } z \geq z_d \text{ in zone 2,} \\ \phi_2^\downarrow \in [\phi_{2m}, \phi_2^M] & \text{for } z < z_d \text{ in zone 2,} \\ 0 & \text{in zone 1 and the underflow zone.} \end{cases} \quad (3.3)$$

Here, ϕ_3 denotes a constant value in zone 3, ϕ_{3M} is the minimum point of the flux function $j_3(\phi)$ in zone 3, and ϕ_2^\uparrow and ϕ_2^\downarrow denote the values above and below, respectively, a discontinuity located at $z = z_d$ within zone 2. For the solids, the following steady state is the most interesting one:

$$\varphi_{SS}(z) := \begin{cases} 0 & \text{in the effluent zone and zones 2 and 3,} \\ \varphi_1 \in [0, \varphi_{1m}] & \text{in zone 1} \\ \varphi_U = \varphi_1 + A_U f_b(\varphi_1)/Q_U & \text{in the underflow zone.} \end{cases} \quad (3.4)$$

The necessary conditions for these steady states to exist involve the following conditions, where we now write out the dependencies on the volumetric flow rates; see (2.9). The conservation of mass across the feed and wash water levels yields the following jump conditions:

$$Q_F \phi_F = A_E j_2(\phi_2; q_2), \quad (\text{FJC})$$

$$Q_F \phi_{s,F} = A_U f_1(\varphi_1, 0; q_1), \quad (\text{FJCs})$$

$$A_E j_2(\phi_2; q_2) = A_E j_3(\phi_3; q_3). \quad (\text{WJC})$$

(Since $\varphi_{SS} = 0$ above and below $z = z_W$, the jump condition there for the solid phase is always satisfied.) For ϕ_{SSd} , ϕ_2 should be replaced by ϕ_2^\downarrow in (FJC) and by ϕ_2^\uparrow in (WJC). We note that for given feed volume fractions ϕ_F and $\phi_{s,F}$, and volumetric flows Q_U and Q_F , the values ϕ_2 (or ϕ_2^\downarrow or ϕ_2^\uparrow) and φ_1 are uniquely given by (FJC) and (FJCs), respectively, for the restrictions given in the solutions (3.1)–(3.4). Then Q_W is given as the unique solution of the following equation (cf. (FJC) and (WJC)):

$$A_E j_3\left(\phi_M\left(\frac{-Q_U + Q_F + Q_W}{A_E}\right); \frac{-Q_U + Q_F + Q_W}{A_E}\right) = Q_F \phi_F. \quad (3.5)$$

Then $\phi_3 = \phi_{3M}(q_3)$ is uniquely determined. The choices of Q_U and Q_F are given by (some of, depending on the steady state) the following inequalities:

$$A_E j_2(\phi_2^M(q_2); q_2) \geq Q_F \phi_F, \quad (\text{FIa})$$

$$\phi_2 \leq \phi_{1Z}(q_1), \quad \text{where } \phi_2 \leq \phi_2^M(q_2) \text{ is defined by (FJC),} \quad (\text{FIb})$$

$$A_E j_2(\phi_{2M}(q_2); q_2) \leq Q_F \phi_F, \quad (\text{FIIa})$$

$$\phi_2 \leq \phi_{1Z}(q_1), \quad \text{where } \phi_2 \in [\phi_2^M(q_2), \phi_{2M}(q_2)] \text{ is defined by (FJC),} \quad (\text{FIIb})$$

$$Q_U > Q_F(1 - \phi_F), \quad (\text{CFIIIa})$$

$$A_U f_1(\varphi_{1M}(q_1), 0; q_1) \geq Q_F \phi_{s,F}. \quad (\text{FIas})$$

Condition (CFIIIa) implies that the wash water injected at the rate Q_W given by (3.5) is effective in the meaning that it flows downwards through the foam. Furthermore, $Q_E > 0$.

3.2. Operating charts.

Case SSI: ϕ_{SS1} and φ_{SS} . The necessary conditions are (FIa), (FIb), (FIas) and (CFIIIa) along with the jump conditions. The first four conditions involve only Q_U and Q_F , and these conditions are visualized in Figure 4 for $\phi_F = 0.3$ and $\phi_{s,F} = 0.1$. The white region in the fifth subplot of Figure 4 shows the possible values for (Q_U, Q_F) . In each such point, there is

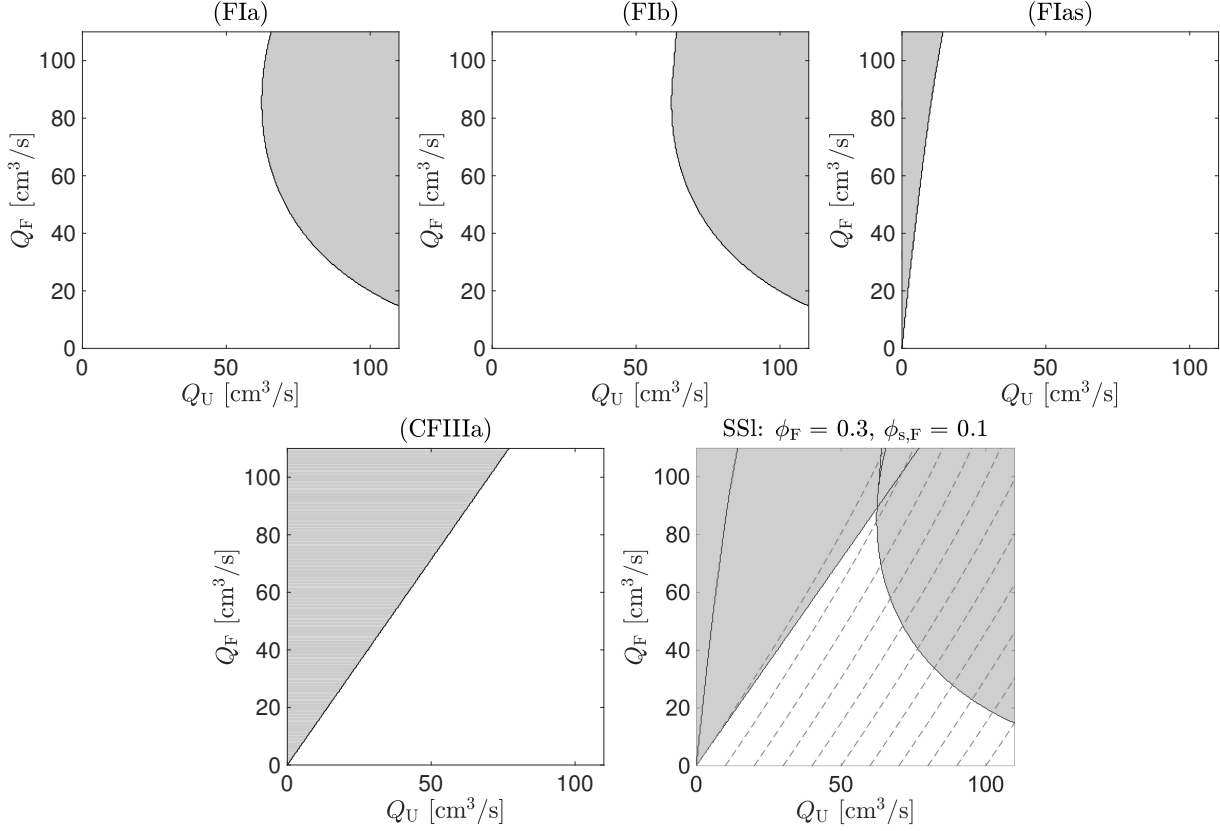


FIGURE 4. Operating charts in the case SS1 with $\phi_F = 0.3$ and $\phi_{s,F} = 0.1$. The four first plots show where each condition is satisfied (white regions). The last plot shows all four conditions superimposed and curves (dashed) along which Q_W is constant with $Q_W = 0, 10, 20, \dots$ cm^3/s . The value of Q_W can be read off on the Q_U -axis.

unique value of Q_W . In the fifth subplot of Figure 4, we have drawn red dashed curves; each for a fixed value of $Q_W = 0, 10, 20, \dots$ cm^3/s , defined by (3.5). The value of Q_W for a specific curve can be read off at the intersection of the curve with the Q_U -axis. This is because $Q_F = 0$ in (3.5) gives $\phi_M((-Q_U + Q_W)/A_U) = \phi_{\max}$, which is equivalent to $Q_W = Q_U$.

Case SS_h: ϕ_{SSh} and φ_{SS} . The conditions are (FIa), (FIIa), (FIIf), (FIas) and (CFIIIa) and the jump conditions. For $\phi_F = 0.3$ and $\phi_{s,F} = 0.1$ we get the regions shown in Figure 5, where we show the new conditions that are not shown in Figure 4.

Case SS_d: ϕ_{SSd} and φ_{SS} . The necessary conditions for this solution are the same as in case SS11b, hence the operating charts coincide with those in Figure 5.

4. NUMERICAL SIMULATIONS

4.1. Preliminaries. In our examples we will use the measures of the flotation column that is part of the Reflux Flotation Cell used by Dickinson and Galvin (2014) and Galvin and

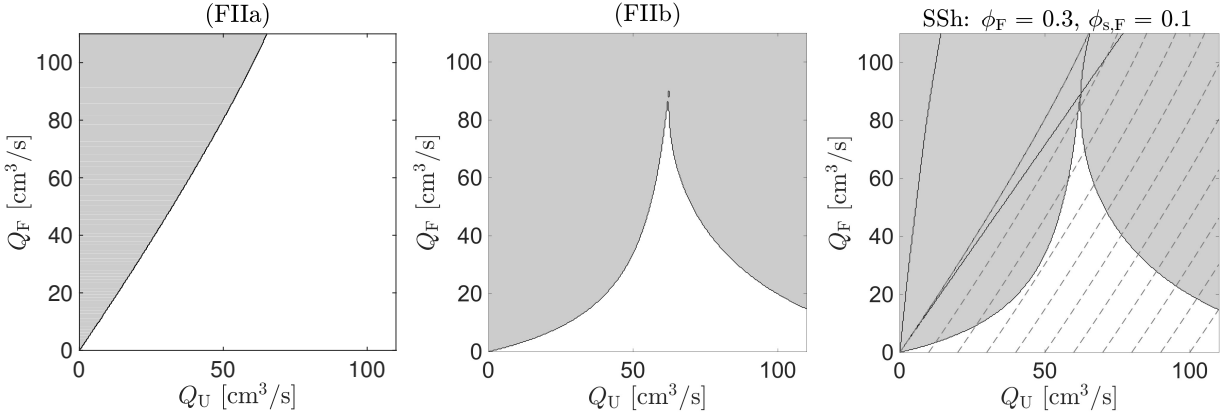


FIGURE 5. Operating charts in the cases SSH and SSD with $\phi_F = 0.3$ and $\phi_{s,F} = 0.1$. The conditions (FIIa) and (FIIb) are shown (see Figure 4 for the others), and in the third plot all conditions together with the dashed lines showing the values of $Q_W = 0, 10, 20, \dots \text{ cm}^3/\text{s}$.

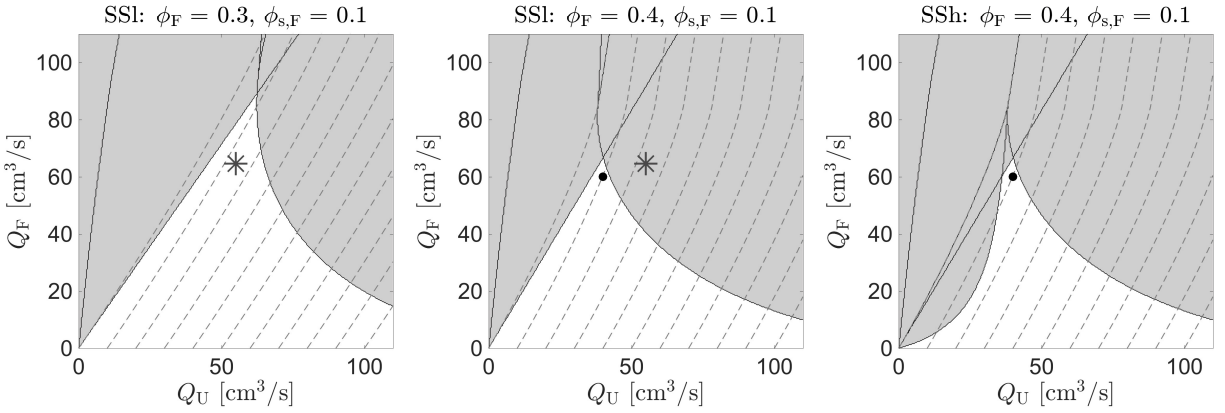


FIGURE 6. Examples 1 and 3. Operating charts for a steady state of type SSL with $\phi_F = 0.3$, $\phi_{s,F} = 0.1$ (left) and $\phi_F = 0.4$, $\phi_{s,F} = 0.1$ (middle) and for a steady state of type SSH with $\phi_F = 0.4$, $\phi_{s,F} = 0.1$ (right). The point $(Q_U, Q_F) = (55, 64.6) \text{ cm}^3/\text{s}$ is marked using a star while $(Q_U, Q_F) = (40, 60) \text{ cm}^3/\text{s}$ is marked with a dot. The dashed curves correspond to constant values of $Q_W = 0, 10, 20, \dots \text{ cm}^3/\text{s}$ where the washing process is effective.

Dickinson (2014). The flotation column is $H = 1 \text{ m}$ high with $A_U = 83.65 \text{ cm}^2$. Feed slurry and gas bubbles are pumped through a downcomer of external diameter 3.81 cm , which forms an annulus around a 2.54 cm -diameter tube incorporating a porous sparger for bubble creation. Hence, the effective horizontal cross-sectional area above the feed inlet is $A_E = 72.25 \text{ cm}^2$. The outlet of the downcomer is positioned 66.7 cm below the top of the vessel, hence a vertical distance of 33.3 cm separates the downcomer outlet from the bottom of the column.

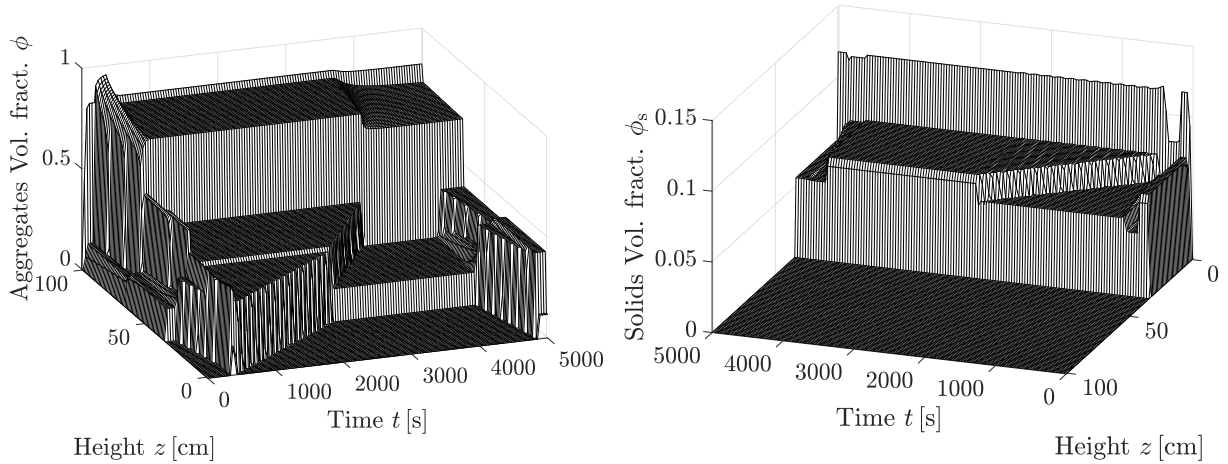


FIGURE 7. Example 1. Time evolution during the first 5000s of the volume fraction profiles of aggregates ϕ (left) and solids ϕ_s (right).

4.2. **Example 1.** We start from a tank filled only with fluid at time $t = 0$ s, where we start pumping aggregates, solids, fluid and wash water, with $\phi_F = 0.3$ and $\phi_{s,F} = 0.1$. From the corresponding operating chart, see Figure 6 (left), we choose the operating point of volumetric flows $(Q_U, Q_F) = (55, 64.6)$ cm³/s lying in the white region and choose $Q_W = 14$ cm³/s by (3.5) to guarantee effective washing, i.e., this is the maximum flow of wash water injected that will flow downwards; applying a higher value will mean an overflow through the effluent. Then a steady-state of type SS1 is feasible with the effluent volumetric flow $Q_E = 25.6$ cm³/s.

Figure 7 shows the first 5000 s of the simulation, while enlarged views are shown in Figure 8. As can be seen in Figure 8 (a) and (b), a first steady state arises after about $t = 100$ s with a low concentration of aggregates in zones 2 and 3; hence, there is no foam and this is an undesired solution. To obtain the desired steady state ϕ_{SS1} , we ‘close’ the top of the tank at $t = 150$ s by setting $Q_U = Q_F + Q_W = 78.6$ cm³/s so that $Q_E = 0$ cm³/s. Then aggregates accumulate at the top forming a layer of foam which grows downwards. The aggregates interact with the solid phase in zone 1 and, eventually, leave through the underflow outlet. At $t = 350$ s, the top of the column is opened again and a desired steady state of type SS1 is reached slowly after $t = 4500$ s; see Figure 7.

Once the system is in steady state, we change, at $t = 4500$ s, the feed volume fraction of aggregates from $\phi_F = 0.3$ to 0.4, and simulate the reaction of the system. In the corresponding operating chart for this new set of variables, the point $(Q_U, Q_F) = (55, 64.6)$ cm³/s is no longer in the white region; see Figure 6 (middle), and no steady state of type SS1 is feasible.

As it can be seen in Figure 8 (c) and (d), the aggregates fill the column downwards through zones 2 and 1 until they leave the tank through the underflow outlet, reaching a non-desired steady state after $t = 5000$ s.

Once this new steady state is reached, we change, at $t = 5000$ s, the volumetric flows so that the new point $(Q_U, Q_F) = (40, 60)$ cm³/s lies inside the white region of the corresponding operating chart in Figure 6 (middle), with $Q_W = 10.2$ cm³/s given by (3.5). Figure 9 shows

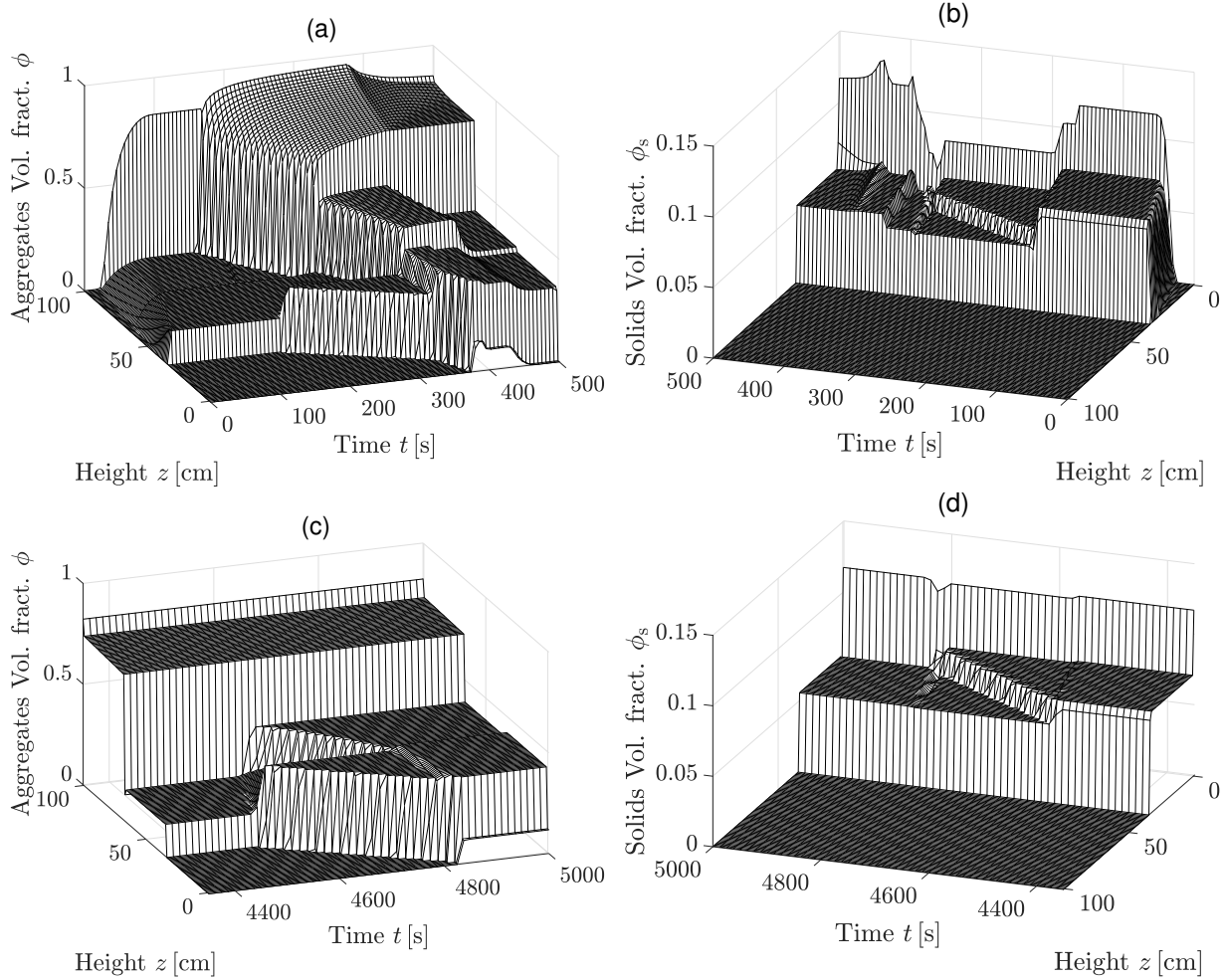


FIGURE 8. Example 1. Enlarged views of the time evolution of the volume fraction profiles of aggregates ϕ in (a) and (c), and solids ϕ_s in (b) and (d), from time $t = 0$ s to 500 s in the upper row and from time $t = 4350$ s to 5000 s in the bottom row.

that a second steady state of type SS1 is slowly reached after $t = 16000$ s. The entire simulation is shown in Figure 10.

4.3. Example 2. Given the same inputs as in Example 1, we let the simulation run until $t = 4500$ s when the feed volume fraction ϕ_F made a step increase from 0.3 to 0.4. Instead of waiting with a control action to $t = 5000$ s (as in Example 1), we now make the control action directly at $t = 4500$ s by setting the volumetric flows to the same values as in Example 1: $(Q_U, Q_F, Q_W) = (40, 60, 10.2)$ cm³/s. The same steady state of type SS1 is quickly reached at about $t = 6500$ s; see Figure 11. The dynamics of the entire simulation can be found in Figure 12.

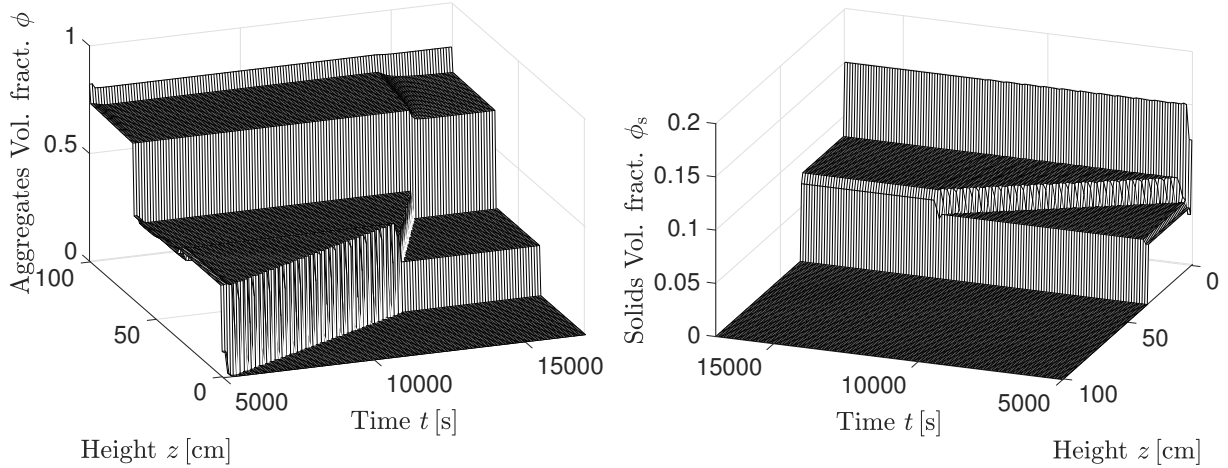


FIGURE 9. Example 1. Time evolution of the volume fraction profiles of aggregates ϕ (left) and solids ϕ_s (right), from time $t = 5000$ s to $t = 17000$ s, when a second steady state is reached.

4.4. **Example 3.** We will demonstrate the cases SSd and SSsh. In Figure 6 (middle) and (right), we see that the point (Q_U, Q_F) lies in the white regions of both feasible steady states SS1 and SSsh (and SSd). We consider the simulation in Example 1 up to $t = 4500$ s when a first desired steady state of type SS1 is reached. At that time point, we close the top of the tank for a short period until $t = 4515$ s, when we simultaneously change the feed volume fraction of aggregates from $\phi_F = 0.3$ to 0.4 and adjust the volumetric flows as in Example 1. It can be seen in Figure 13 that a steady state of type SSd is reached after just $t = 5000$ s, with a stationary discontinuity in zone 2 at $z_d \approx 46$ cm, above and below which the volume fractions are

$$\begin{cases} \phi_2^\uparrow = 0.3621 \in [\phi_2^M, \phi_{2M}] = [0.2899, 0.7490] & \text{for } z > z_d, \\ \phi_2^\downarrow = 0.2283 \in [\phi_{2m}, \phi_2^M] = [0.1078, 0.2899] & \text{for } z < z_d, \end{cases}$$

satisfying $j_2(\phi_2^\uparrow) = j_2(\phi_2^\downarrow)$.

Analogously, if we perform the same actions except that the top is closed for 21 s instead of 15 s, then a steady state of type SSsh is reached after $t = 5000$ s; see Figure 14.

5. CONCLUSIONS AND DISCUSSIONS

The present study outlines a model of a flotation column that is consistent with the old drift- and solids-flux theories, which have been proposed separately for the bubble-liquid subsystem of a flotation column and for the settling of particles. The mathematical and numerical analysis provides a framework that complements the flux constructions done in some recent papers (Vandenberghe et al. 2005; Stevenson et al. 2008; Dickinson and Galvin 2014; Galvin and Dickinson 2014) and leads to a simple but formally complete model of steady states and transient operation of the flotation column. The novelty of the approach (for the application to flotation) consists in the implementation of recently developed knowledge on the determination and well-posedness of solutions to conservation laws with discontinuous

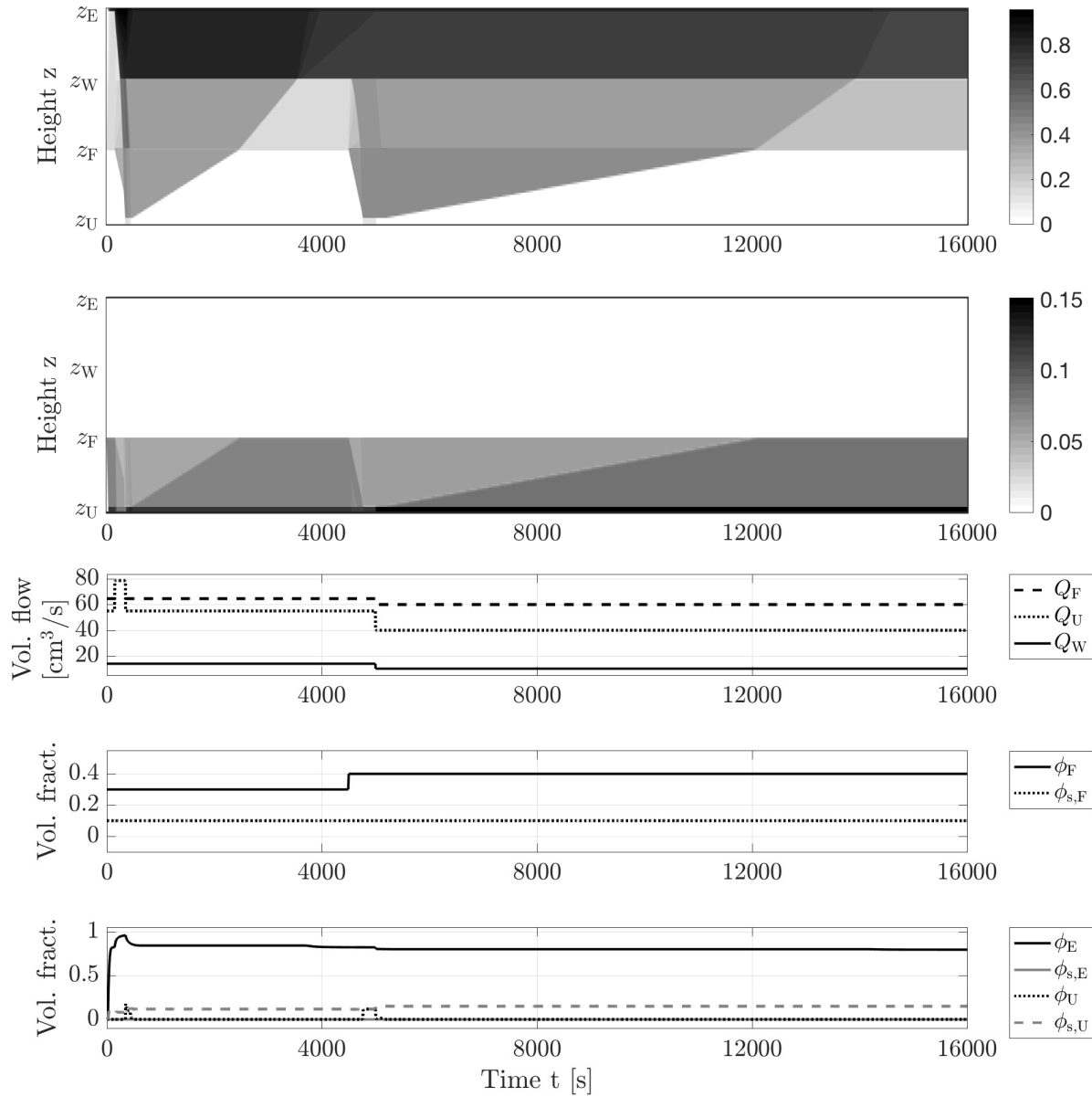


FIGURE 10. Example 1. Dynamics of the entire simulation during 16000 s. Here and in Figure 12, the panels show (from top to bottom) the aggregate volume fraction ϕ ; the solids volume fraction ϕ_s ; the volumetric flows Q_U , Q_F and Q_W ; the volume fractions of aggregates and solids of the feed (ϕ_F and $\phi_{s,F}$); and the volume fractions of aggregates and solids of the underflow (ϕ_U and $\phi_{s,U}$) and the effluent (ϕ_E and $\phi_{s,E}$).

flux. While some of the mathematical details and a complete classification of steady states are beyond the scope of the paper (but see Bürger et al. 2019), the benefits of the approach should become clear through the consistency between the operating charts and the response

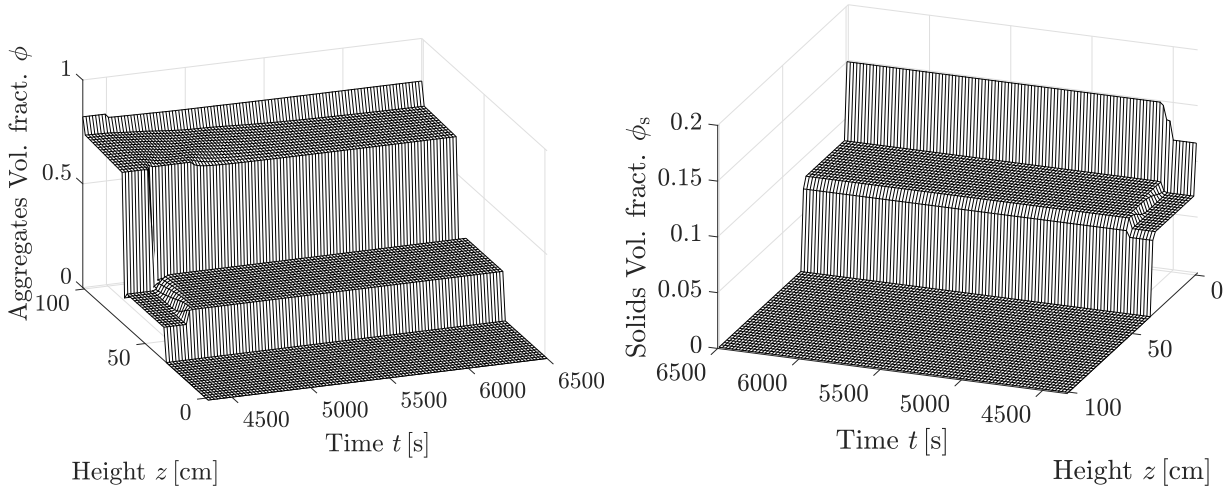


FIGURE 11. Example 2. Time evolution of the volume fraction profiles of aggregates ϕ (left) and solids ϕ_s (right) from time $t = 4350$ s to $t = 6500$ s.

of the system to changes in the feed inputs and control actions. That said, we emphasize that the steady states and the nonlinear conditions behind the operating charts in Section 3 are valid to *any* pair of functions j_b and f_b that satisfy the assumptions in Section 2.4. Of course, the operating charts, and in particular the existence, size, and shape of the region of feasibility of the different steady states (the “white regions” of the fifth plot of Figure 4, the third plot of Figure 5, and the plots of Figure 6) depend on the particular choices of j_b and f_b . In the same spirit we mention that the flotation column has been subdivided into three zones of equal height (zones 1, 2 and 3) for illustrative purposes only; the model allows any sizes of the zones.

In most applications, the adhesion of hydrophobic particles to bubbles takes place in the collection region shown in Figure 1 (b). This is a region of countercurrent flow: bubbles move upward and solid particles settle (Bergh and Yianatos 2003; Yianatos et al. 2005) while the attachment of hydrophobic particles to bubbles occurs. In future work, we will extend the model described by (1.1) into one that accounts for the aggregation process. This requires including reaction terms. In addition, a separate PDE needs to be introduced for a third field variable, for instance the number of solid particles attached to a single bubble at each spatial position and time. The resulting 3×3 convection-reaction system is likely to form a model that could be used for design and control simulations (so-called model-predictive control; see Bergh and Yianatos 1995, 2011; Maldonado et al. 2009).

Finally, we recall that the present model is a quasilinear first-order system of conservation laws, whose solutions, that is the profiles of ϕ , φ and ϕ_s are in general discontinuous, both stationary ones at the boundary between zones and possibly moving ones within zones. The latter property is easily visible in the sharp discontinuities that travel at non-constant speed; see Figures 7 to 14. However, the simulation model could still be augmented by diffusion terms (i.e., terms involving second derivatives of the unknowns with respect to z) to account for constant, local or nonlinear axial dispersion (as suggested, for instance, by Mills and

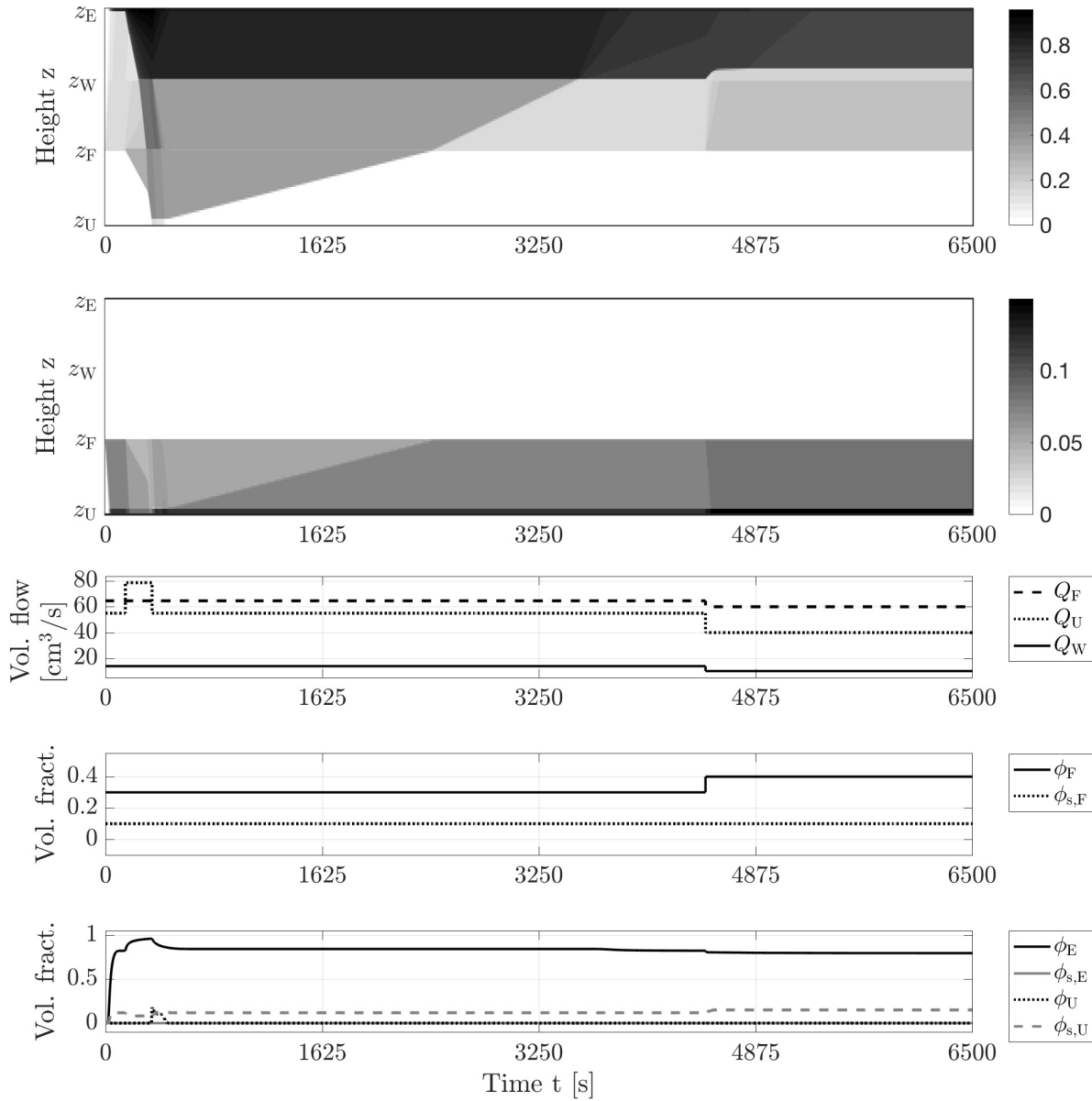


FIGURE 12. Example 2. Dynamics of various variables from the initial time $t = 0$ s to $t = 6500$ s.

O'Connor 1990; Newcombe 2014; Gharai and Venugopal 2016), convective-dispersive gangue transport (Stevenson et al. 2007), or strongly degenerate diffusion describing compressibility of the foam layer (Narsimhan 2010). The effect of axial dispersion will be a blurring of otherwise sharp interfaces.

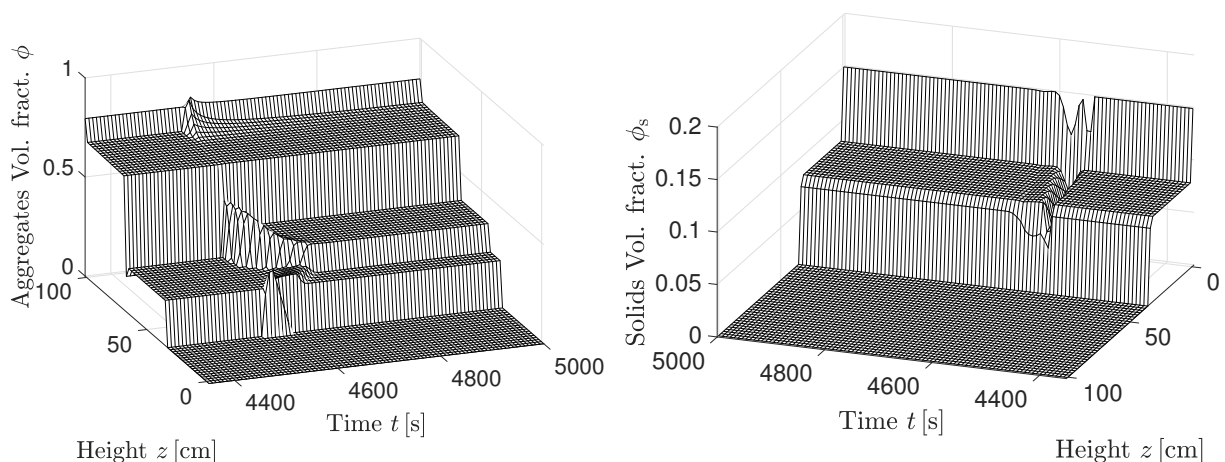


FIGURE 13. Example 3. Transient solution between the steady states SS_l and SS_d, where the latter has a discontinuity in the aggregate volume fraction in zone 2.

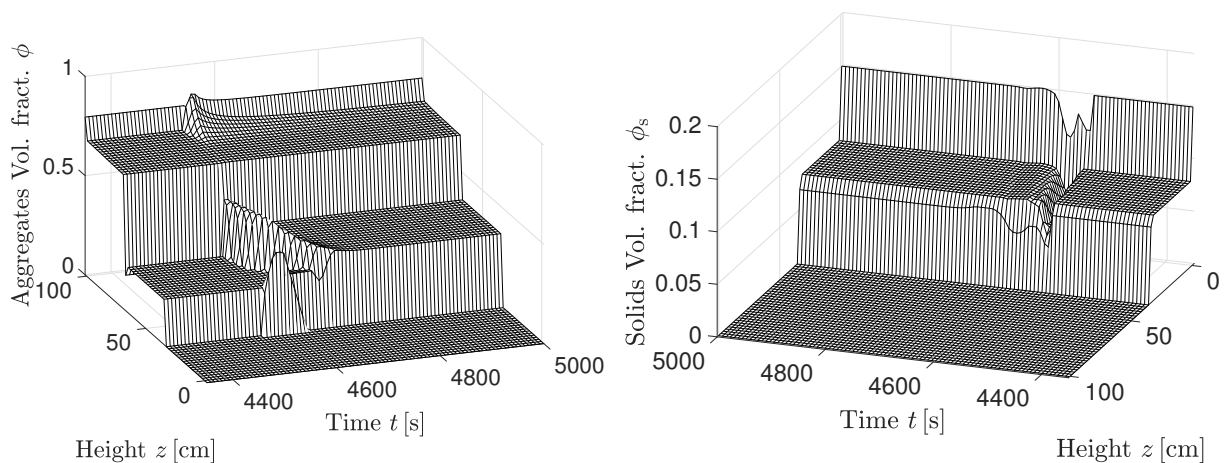


FIGURE 14. Example 3. Transient solution between the steady states SS_l and SS_h.

ACKNOWLEDGMENTS

R.B. acknowledges support by Fondecyt project 1170473; CONICYT/PIA/Concurso Apoyo a Centros Científicos y Tecnológicos de Excelencia con Financiamiento Basal AFB170001; CRHIAM, Project CONICYT/FONDAP/15130015; and by the INRIA Associated Team “Efficient numerical schemes for non-local transport phenomena” (NOLOCO; 2018–2020). M.C.M. is supported by Spanish MINECO grant MTM2017-83942-P. Y.V. is supported by SENACYT (Panama).

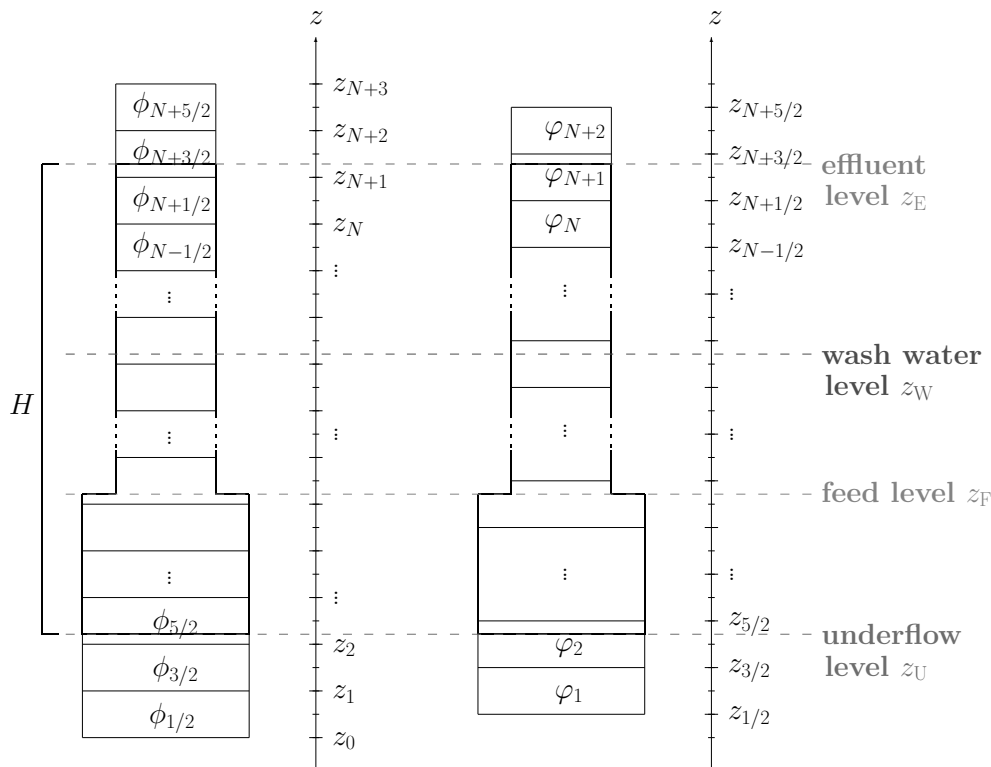


FIGURE 15. Two staggered grids for the discretization of the flotation column with the spatial discontinuities away from cell boundaries.

APPENDIX: NUMERICAL SCHEME

The discretization of the model exploits that the system of balance laws (1.1) is triangular. Bürger et al. (2019) describe the numerical scheme and we have a proof (still unpublished) that the numerical volume fractions stay between zero and one. The scheme uses a staggered grid for the two unknown functions ϕ and φ of (1.1). The Godunov method (Godunov, 1959) is used first to obtain a piecewise constant, in space and time, approximation of the solution ϕ of (1.1a). Then the updated ϕ -values are used as a given piecewise constant function in (1.1b). By using a staggered grid for the numerical approximation of φ , we achieve that the Godunov flux is well defined. For the same reason, the two grids should preferably be placed so that the known spatial discontinuities at z_U , z_F , z_W and z_E lie inside cells of both grids.

Spatial discretization. We let N cells for each grid cover the column, so that cell 1 contains z_U and cell N contains z_E ; see Figure 15. We add extra cells at the bottom and top to calculate the outlet volume fractions. We define $\Delta z := H/(N - 1)$, where H is the height of the column from the underflow level z_U to the effluent level z_E , $z_i := (i - 2)\Delta z$, $i = 0, 1/2, 1, 3/2, \dots, N + 3$, so that $z_U = z_2 + \Delta z/4$ and $z_E = z_{N+1} + \Delta z/4$. Each of the injection points z_F and z_W will belong to one interval of each grid. The numerical method

implicitly assumes that these two locations are placed a distance $\Delta z/4$ from the nearest boundary of both grids.

The cross-sectional area $A = A(z)$, which is allowed to have a finite number of discontinuities, is discretized by cell-wise averages, namely we calculate

$$A_{i+1/2} := \frac{1}{\Delta z} \int_{z_i}^{z_{i+1}} A(z) dz, \quad A_i := \frac{1}{\Delta z} \int_{z_{i-1/2}}^{z_{i+1/2}} A(z) dz. \quad (\text{A.1})$$

Furthermore, we determine from these values the constants

$$M := \max \left\{ \frac{A_{i-1/2}}{A_i}, \frac{A_{i+1/2}}{A_i} : i = 1, \frac{3}{2}, \dots, N + \frac{3}{2}, N + 2 \right\}, \quad (\text{A.2})$$

$$A_{\min} := \min \{ A_{1/2}, A_1, \dots, A_{N+1}, A_{N+3/2} \}. \quad (\text{A.3})$$

Time discretization. We use the uniform step length Δt and simulate N_T time steps up to the final time $T := N_T \Delta t$, and we set $t_n := n \Delta t$ for $n = 0, 1, \dots, N_T$. The time step Δt should satisfy the Courant-Friedrichs-Lewy (CFL) condition

$$\Delta t M \left(\|j'_b\|_\infty + \|f'_b\|_\infty + \frac{\|Q\|_\infty}{A_{\min}} \right) \leq \frac{\Delta z}{2}, \quad (\text{A.4})$$

where the constants are given by (A.2), (A.3) and

$$\begin{aligned} \|j'_b\|_\infty &:= \max_{0 \leq \phi \leq 1} |j'_b(\phi)|, \\ \|f'_b\|_\infty &:= \max_{0 \leq \varphi \leq 1} |f'_b(\varphi)|, \\ \|Q\|_\infty &:= \max_{0 \leq t \leq T} (Q_F(t) + Q_W(t)). \end{aligned}$$

The CFL condition (A.4) is a well-known stability condition that usually arises in the context of explicit discretizations of time-dependent partial differential equations (see, e.g., LeVeque, 1992) and limits Δt for given Δz .

The time-dependent feed functions are discretized as

$$Q_F^n := \frac{1}{\Delta t} \int_{t_n}^{t_{n+1}} Q_F(t) dt, \quad \phi_F^n := \frac{1}{\Delta t} \int_{t_n}^{t_{n+1}} \phi_F(t) dt,$$

and the same is made for the other volumetric flows and $\phi_{s,F}$.

Marching formula. Assume that Δz is the spatial mesh width (“layer thickness”) specified above and Δt is the time step chosen such that (A.4) is in effect. To state the marching (update) formula that constitutes the numerical scheme, we define the dimensionless symbol

$$\delta_{F,i+1/2} := \int_{z_i}^{z_{i+1}} \delta_{z_F}(z) dz := \begin{cases} 1 & \text{if } z_F \in [z_i, z_{i+1}), \\ 0 & \text{otherwise.} \end{cases}$$

The numerical approximations of the PDE solutions are denoted by $\phi_{i+1/2}^n \approx \phi(z_{i+1/2}, t_n)$ and $\varphi_i^n \approx \varphi(z_i, t_n)$. More precisely, the initial data are discretized by

$$\phi_{i+1/2}^0 := \frac{1}{A_{i+1/2} \Delta z} \int_{z_i}^{z_{i+1}} \phi(z, 0) A(z) dz, \quad \varphi_i^0 := \frac{1}{A_i \Delta z} \int_{z_{i-1/2}}^{z_{i+1/2}} \varphi(z, 0) A(z) dz,$$

and the scheme (marching formula) is

$$\phi_{i+1/2}^{n+1} = \phi_{i+1/2}^n + \frac{\Delta t}{A_{i+1/2}\Delta z} (A_i \mathcal{J}_i^n - A_{i+1} \mathcal{J}_{i+1}^n + Q_F^n \phi_F^n \delta_{F,i+1/2}),$$

$$\varphi_i^{n+1} = \begin{cases} \varphi_i^n & \text{if } \phi_{i-1/2}^n + \phi_{i+1/2}^n = 2, \\ \varphi_i^n + \frac{\Delta t (A_{i-1/2} \mathcal{F}_{i-1/2}^n - A_{i+1/2} \mathcal{F}_{i+1/2}^n + Q_F^n \phi_{s,F}^n \delta_{F,i})}{(1 - (\phi_{i-1/2}^n + \phi_{i+1/2}^n)/2)\Delta z A_i} & \text{otherwise,} \end{cases}$$

where \mathcal{J}_i^n and $\mathcal{F}_{i+1/2}^n$ are numerical flux values arising by suitable applications of the numerical flux by Godunov (1959), namely

$$\mathcal{J}_i^n = \begin{cases} \min_{\phi_{i-1/2}^n \leq \phi \leq \phi_{i+1/2}^n} J(\phi, z_i, t_n) & \text{if } \phi_{i-1/2}^n \leq \phi_{i+1/2}^n, \\ \max_{\phi_{i-1/2}^n \geq \phi \geq \phi_{i+1/2}^n} J(\phi, z_i, t_n) & \text{if } \phi_{i-1/2}^n > \phi_{i+1/2}^n, \end{cases} \quad (\text{A.5})$$

$$\mathcal{F}_{i+1/2}^n = \begin{cases} - \min_{\varphi_{i+1}^n \leq \varphi \leq \varphi_i^n} F(\varphi, \phi_{i+1/2}^n, z_{i+1/2}, t_n) & \text{if } \varphi_{i+1}^n \leq \varphi_i^n, \\ - \max_{\varphi_{i+1}^n \geq \varphi \geq \varphi_i^n} F(\varphi, \phi_{i+1/2}^n, z_{i+1/2}, t_n) & \text{if } \varphi_{i+1}^n > \varphi_i^n. \end{cases} \quad (\text{A.6})$$

In the numerical flux \mathcal{J}_i^n , we replace $A(z_i)$ by A_i , and analogously for $\mathcal{F}_{i+1/2}^n$.

Once $\phi_{i+1/2}^{n+1}$ and φ_i^{n+1} have been calculated, we define an approximate solution for the solids volume fraction ϕ_s by

$$\phi_{s,i}^{n+1} := \left(1 - \frac{\phi_{i-1/2}^n + \phi_{i+1/2}^n}{2}\right) \varphi_i^{n+1} \quad \text{for all } i, n.$$

NOMENCLATURE

Latin symbols

$A(z)$	cross-sectional area of the column at height z [cm ²]
$A_i, A_{i+1/2}$	cell averages of $A(z)$, defined in (A.1) [cm ²]
A_{\min}	constant defined in (A.3) [cm ²]
A_U, A_E	cross-sectional area below/above feed level (cf. Figure 2) [cm ²]
f	generic solids zone flux function (Section 2.4) [cm/s]
f_E	effluent solids zone flux function [cm/s]
f_U	underflow solids zone flux function [cm/s]
f_1, f_2, f_3	solids zone flux function in zone 1, 2, 3 [cm/s]
f_b	batch solids-flux function [cm/s]
$F(\varphi, \phi, z, t)$	flux of the solids balance equation (1.1b) [cm/s]
$\mathcal{F}_{i+1/2}^n$	value of numerical flux defined by (A.6) [cm/s]
H	column height [cm]
j	generic aggregates zone flux function (Section 2.4) [cm/s]
j_1, j_2, j_3	aggregates zone flux function in zone 1, 2, 3 [cm/s]
j_b	batch drift-flux function [cm/s]
j_E	effluent aggregates zone flux function [cm/s]
j_U	underflow aggregates zone flux function [cm/s]

$J(\phi, z, t)$	flux of the aggregates balance equation (1.1a) [cm/s]
\mathcal{J}_i^n	value of numerical flux defined by (A.5) [cm/s]
M	constant defined in (A.2) [-]
n_a, n_s	Richardson-Zaki exponents in (2.4) [-]
N	number of cells covering column in the numerical method [-]
N_T	number of time steps in numerical method [-]
q	bulk velocity of the mixture [cm/s]
q_1, q_2, q_3	bulk velocity of the mixture in zone 1, 2, 3 [cm/s]
q_{sus}	bulk velocity of the solid-fluid suspension [cm/s]
Q_E	volumetric effluent flow [cm ³ /s]
Q_F	volumetric feed flow [cm ³ /s]
Q_F^n	discrete value of Q_F [cm ³ /s]
Q_U	volumetric underflow [cm ³ /s]
Q_W	volumetric wash water feed rate [cm ³ /s]
t	time [s]
t_n	time after n time steps [s]
T	final simulation time [s]
u_{asus}	aggregates-suspension relative velocity [cm/s]
u_{sf}	solid-fluid relative velocity [cm/s]
v_a	aggregates phase velocity [cm/s]
v_f	fluid phase velocity [cm/s]
v_s	solids phase velocity [cm/s]
$V_a(\phi)$	dimensionless hindered bubbling function [-]
$V_s(\varphi)$	dimensionless hindered settling function [-]
z	height [cm]
z_d	discontinuity in zone 2, see (3.3) [cm]
z_E	effluent level [cm]
z_F	feed level [cm]
z_U	underflow level [cm]
z_W	wash water feed level [cm]

Greek symbols

$\delta(\cdot)$	Dirac delta function [cm ⁻¹]
$\delta_{F,i+1/2}$	dimensionless symbol associated with feed level [-]
Δt	time step [s]
Δz	spatial meshwidth [cm]
ϕ	volume fraction of bubbles [-]
ϕ_1, ϕ_2, ϕ_3	steady-state values of ϕ in zones 1, 2, 3 [-]
$\phi_2^\uparrow, \phi_2^\downarrow$	steady-state values of ϕ adjacent to z_d (see (3.3)) [-]
$\phi_{i+1/2}^n$	approximate value of $\phi(z_{i+1/2}, t_n)$ [-]
$\phi_F(t)$	feed volume fraction of aggregates at time t [-]
ϕ_F^n	discrete value of ϕ_F at time t_n [-]
ϕ_{infl}	inflection point of j and j_b [-]
ϕ_m	ϕ -value satisfying $\phi_m \leq \phi_{\text{infl}}$ and $j(\phi_m) = j(\phi_M)$, see (2.12) [-]

$\phi_{1m}, \phi_{2m}, \phi_{3m}$	values of ϕ_m in zones 1, 2, 3 [-]
ϕ_M	local minimum of j in interval $(\phi_{\text{infl}}, 1)$ [-]
$\phi_{1M}, \phi_{2M}, \phi_{3M}$	values of ϕ_M in zones 1, 2, 3 [-]
ϕ^M	local maximum of j in $[0, \phi_{\text{infl}})$ [-]
$\phi_1^M, \phi_2^M, \phi_3^M$	values of ϕ^M in zones 1, 2, 3 [-]
$\phi_{s,F}(t)$	feed volume fraction of solids at time t [-]
$\phi_{s,F}^n$	discrete value of $\phi_{s,F}$ at time t_n [-]
ϕ_s	volume fraction of solids [-]
$\phi_{SSl}, \phi_{SSh}, \phi_{SSd}$	steady state profile of ϕ with low, high, or discontinuous value in zone 2 [-]
ϕ_Z	zero of $j(\phi)$ [-]
φ	volume fraction of solids in solid-liquid suspension [-]
φ_1	steady-state value of φ in zone 1 [-]
φ_U	steady-state value of φ in underflow zone [-]
φ_i^n	approximate value of $\varphi(z_i, t_n)$ [-]
$\varphi_{SS}(z)$	steady-state profile for φ [-]
ρ_a, ρ_f, ρ_s	density of aggregates, fluid, and solids [g/cm ³]

REFERENCES

- Bascur, O.A., 1991, "A unified solid/liquid separation framework." *Fluid/Particle Separation Journal*, 4, pp. 117–122.
- Bergh, L.G. and Yianatos, J.B., 1995, "Dynamic simulation of operating variables in flotation columns." *Minerals Engineering*, 8, pp. 603–613.
- Bergh, L.G. and Yianatos, J.B., 2003 "Flotation column automation: state of the art." *Control Engineering and Practice*, 11, pp. 67–72.
- Bergh, L.G. and Yianatos, J.B., 2011, "The long way to multivariate predictive control of flotation processes." *Journal of Process Control*, 21, pp. 226–234.
- Brennen, C.E., 2005, *Fundamentals of Multiphase Flow* Cambridge, UK; Cambridge University Press.
- Bürger, R., Karlsen, K.H., Risebro, N.H., and Towers, J.D., 2004, "Well-posedness in BV_t and convergence of a difference scheme for continuous sedimentation in ideal clarifier-thickener units." *Numerische Mathematik*, 97, pp. 25–65.
- Bürger, R., Karlsen, K.H., and Towers, J.D., 2005, "A model of continuous sedimentation of flocculated suspensions in clarifier-thickener units." *SIAM Journal on Applied Mathematics*, 65, pp. 882–940.
- Bürger, R., Karlsen, K.H., Torres, H., and Towers, J.D., 2010, "Second-order schemes for conservation laws with discontinuous flux modelling clarifier-thickener units." *Numerische Mathematik*, 116, pp. 579–617.
- Bürger, R., Diehl, S., Farås, S., Nopens, I., and Torfs, E., 2013, "A consistent modelling methodology for secondary settling tanks: a reliable numerical method." *Water Science and Technology*, 68, pp. 192–208.

- Bürger, R., Diehl, S., and Martí, M.C., 2018a, “A conservation law with multiply discontinuous flux modelling a flotation column.” *Networks and Heterogeneous Media*, 13, pp. 339–371.
- Bürger, R., Diehl, S., and Mejías, C., 2018b, “A difference scheme for a degenerating convection-diffusion-reaction system modelling continuous sedimentation.” *ESAIM: Mathematical Modelling and Numerical Analysis*, 52, pp. 365–392.
- Bürger, R., Diehl, S., and Martí, M.C., 2019, “A system of conservation laws with discontinuous flux modelling flotation with sedimentation.” Preprint 2019-09, Centro de Investigación en Ingeniería Matemática, Universidad de Concepción; submitted.
- Cruz, E.B., 1997, A comprehensive dynamic model of the column flotation unit operation. PhD Thesis, Virginia Tech, Blacksburg, VA.
- Dickinson, J.E. and Galvin, K.P., 2014, “Fluidized bed desliming in fine particle flotation, Part I.”, *Chemical Engineering Science*, 108, pp. 283–298.
- Diehl, S., 1996, “A conservation law with point source and discontinuous flux function modelling continuous sedimentation.”, *SIAM Journal on Applied Mathematics*, 56, pp. 388–419.
- Diehl, S., 2001, “Operating charts for continuous sedimentation I: control of steady states.”, *Journal of Engineering Mathematics*, 41, pp. 117–144.
- Diehl, S., 2005, “Operating charts for continuous sedimentation II: step responses.”, *Journal of Engineering Mathematics*, 53, pp. 139–185.
- Diehl, S., 2008, “The solids-flux theory—confirmation and extension by using partial differential equations.”, *Water Research*, 42, pp. 4976–4988.
- Dobby, G.S., Yianatos, J.B., and Finch, 1988, “Estimation of bubble diameter in flotation columns from drift flux analysis.”, *Canadian Metallurgical Quarterly*, 27, pp. 85–90.
- Finch, J.A. and Dobby, G.S., 1990, *Column Flotation*, 1st edition, London, UK; Pergamon Press.
- Galvin, K.P. and Dickinson, J.E., 2014, “Fluidized bed desliming in fine particle flotation Part II: Flotation of a model feed.”, *Chemical Engineering Science*, 108, pp. 299–309.
- Galvin, K.P., Harvey, N.G., and Dickinson, J.E., 2014, “Fluidized bed desliming in fine particle flotation—part III: flotation of difficult to clean coal.”, *Minerals Engineering* 66–68, pp. 94–101.
- Gharai, M. and Venugopal, R., 2016, Modeling of flotation process—an overview of different approaches.”, *Mineral Processing and Extractive Metallurgy Review*, 37, pp. 120–133.
- Godunov, S.K., 1959, “Finite difference methods for numerical computation of discontinuous solutions of equations of fluid dynamics.”, *Mat. Sbornik*, 47, pp. 271–295.
- Holden, H. and Risebro, N.H., 2015, *Front Tracking for Hyperbolic Conservation Laws*, 2nd edition, Berlin, Germany; Springer Verlag.
- Ireland, P.M. and Jameson, G.J., 2007, “Liquid transport in multi-layer froths.”, *Journal of Colloid and Interface Science*, 314, pp. 207–213.
- Kynch, G.J., 1952, “A theory of sedimentation.”, *Transactions of the Faraday Society*, 48, pp. 166–176.
- Langberg, D.E. and Jameson, G.J., 1992, “The coexistence of the froth and liquid phases in a flotation column.”, *Chemical Engineering Science*, 47, pp. 4345–4355.

- LeVeque, R.J., 1992, *Numerical Methods for Conservation Laws*, Birkhäuser Verlag, Basel, Switzerland, 1992.
- Maldonado, M., Desbiens, A., and del Villar, R., 2009, “Potential use of model predictive control for optimizing the column flotation process.”, *International Journal of Mineral Processing*, 93, pp. 26–33.
- Mills, P.J.T. and O’Connor, C.T., 1990, “The modelling of liquid and solids mixing in a flotation column.”, *Minerals Engineering*, 3, pp. 567–576.
- Narsimhan, G., 2010, “Analysis of creaming and formation of foam layer in aerated liquid.”, *Journal of Colloid and Interface Science*, 345, pp. 566–572.
- Newcombe, B., 2014, “A phenomenological model for an industrial flash flotation cell.”, *Minerals Engineering*, 64, pp. 51–62.
- Pal, R. and Masliyah, J.H., 1989, “Flow characterization of a flotation column.”, *Canadian Journal of Chemical Engineering*, 67, pp. 916–923.
- Richardson, J.F. and Zaki, W.N., “Sedimentation and fluidisation: Part I.”, *Transactions of the Institution of Chemical Engineers (London)*, 32, 34–53.
- Rietema, K., 1982, “Science and technology of dispersed two-phase systems—I and II.”, *Chemical Engineering Science*, 37, pp. 1125–1150.
- Rubio, J., Souza, M.L., and Smith, R.W., 2002, “Overview of flotation as a wastewater treatment technique.”, *Minerals Engineering*, 15, pp. 139–155.
- Stevenson, P., Ata, S., and Evans, G.M., 2007, Convective-dispersive gangue transport in flotation froth, *Chemical Engineering Science*, 62, pp. 5736–5744.
- Stevenson, P., Fennell, P.S., and Galvin, K.P., 2008, “On the drift-flux analysis of flotation and foam fractionation processes.”, *Canadian Journal of Chemical Engineering*, 86, pp. 635–642.
- Tian, Y., Azhin, M., Luan, X., Liu, F., and Dubljevic, S., 2018, “Three-phases dynamic modelling of column flotation process.”, *IFAC-PapersOnLine*, 51, no. 21, pp. 99–104.
- Vandenbergh, J., Chung, J., Xu, Z., and Masliyah, J., 2005, “Drift flux modelling for a two-phase system in a flotation column.”, *Canadian Journal of Chemical Engineering*, 83, pp. 169–176.
- Wallis, G.B., 1969, *One-Dimensional Two-Phase Flow*, 1st edition, New York; McGraw-Hill.
- Yianatos, J.B., Bucarey, R., Larenas, J., Henríquez, F., and Torres, L., 2005, “Collection zone kinetic model for industrial flotation columns.” *Minerals Engineering*, 18, 1373–1377.
- Yianatos, J.B., Finch, J.A., and Laplante, A.R., 1986, “Apparent hindered settling in a gas-liquid-solid countercurrent column.” *International Journal of Mineral Processing*, 18, pp. 155–165.

Centro de Investigación en Ingeniería Matemática (CI²MA)

PRE-PUBLICACIONES 2019

- 2019-14 MARCELO CAVALCANTI, WELLINGTON CORREA, TÜRKER ÖZSARI, MAURICIO SEPÚLVEDA, RODRIGO VÉJAR: *Exponential stability for the nonlinear Schrödinger equation with locally distributed damping*
- 2019-15 RICARDO OYARZÚA, MANUEL SOLANO, PAULO ZUÑIGA: *A priori and a posteriori error analyses of a high order unfitted mixed-FEM for Stokes flow*
- 2019-16 DAVID MORA, IVÁN VELÁSQUEZ: *Virtual element for the buckling problem of Kirchhoff-Love plates*
- 2019-17 VERONICA ANAYA, BRYAN GOMEZ-VARGAS, DAVID MORA, RICARDO RUIZ-BAIER: *Incorporating variable viscosity in vorticity-based formulations for Brinkman equations*
- 2019-18 FELIPE LEPE, DAVID MORA: *Symmetric and non-symmetric discontinuous Galerkin methods for a pseudostress formulation of the Stokes spectral problem*
- 2019-19 ANTONIO BAEZA, RAIMUND BÜRGER, PEP MULET, DAVID ZORÍO: *An efficient third-order WENO scheme with unconditionally optimal accuracy*
- 2019-20 TOMÁS BARRIOS, EDWIN BEHRENS, ROMMEL BUSTINZA: *A stabilised mixed method applied to compressible fluid flow: The stationary case*
- 2019-21 VERONICA ANAYA, ZOA DE WIJN, BRYAN GOMEZ-VARGAS, DAVID MORA, RICARDO RUIZ-BAIER: *Rotation-based mixed formulations for an elasticity-poroelasticity interface problem*
- 2019-22 GABRIEL N. GATICA, SALIM MEDDAHI: *Coupling of virtual element and boundary element methods for the solution of acoustic scattering problems*
- 2019-23 GRAHAM BAIRD, RAIMUND BÜRGER, PAUL E. MÉNDEZ, RICARDO RUIZ-BAIER: *Second-order schemes for axisymmetric Navier-Stokes-Brinkman and transport equations modelling water filters*
- 2019-24 JULIO ARACENA, CHRISTOPHER THRAVES: *The weighted sitting closer to friends than enemies problem in the line*
- 2019-25 RAIMUND BÜRGER, STEFAN DIEHL, MARÍA CARMEN MARTÍ, YOLANDA VÁSQUEZ: *A model of flotation with sedimentation: steady states and numerical simulation of transient operation*

Para obtener copias de las Pre-Publicaciones, escribir o llamar a: DIRECTOR, CENTRO DE INVESTIGACIÓN EN INGENIERÍA MATEMÁTICA, UNIVERSIDAD DE CONCEPCIÓN, CASILLA 160-C, CONCEPCIÓN, CHILE, TEL.: 41-2661324, o bien, visitar la página web del centro: <http://www.ci2ma.udec.cl>



**CENTRO DE INVESTIGACIÓN EN
INGENIERÍA MATEMÁTICA (CI²MA)
Universidad de Concepción**



Casilla 160-C, Concepción, Chile
Tel.: 56-41-2661324/2661554/2661316
<http://www.ci2ma.udec.cl>